

Several fitness functions and entanglement gates in quantum kernel generation

Haiyan Wang*

School of Mathematical and Natural Science, Arizona State University, Phoenix, AZ 85069, USA

Quantum machine learning (QML) represents a promising frontier in the realm of quantum technologies. In this pursuit of quantum advantage, the quantum kernel method for support vector machine has emerged as a powerful approach. Entanglement, a fundamental concept in quantum mechanics, assumes a central role in quantum computing. In this paper, we study the necessities of entanglement gates in the quantum kernel methods. We present several fitness functions for a multi-objective genetic algorithm that simultaneously maximizes classification accuracy while minimizing both the local and non-local gate costs of the quantum feature map's circuit. We conduct comparisons with classical classifiers to gain insights into the benefits of employing entanglement gates. Surprisingly, our experiments reveal that the optimal configuration of quantum circuits for the quantum kernel method incorporates a proportional number of non-local gates for entanglement, contrary to previous literature where non-local gates were largely suppressed.

Furthermore, we demonstrate that the separability indexes of data can be effectively leveraged to determine the number of non-local gates required for the quantum support vector machine's feature maps. This insight can significantly aid in selecting appropriate parameters, such as the entanglement parameter, in various quantum programming packages like <https://qiskit.org/> based on data analysis. Our findings offer valuable guidance for enhancing the efficiency and accuracy of quantum machine learning algorithms.

Keywords: support vector machine; quantum feature map; genetic algorithm; entanglement gate

1. INTRODUCTION

Quantum machine learning (QML) stands out as one of the most promising and fascinating applications of quantum technologies. In this pursuit of quantum advantage, the quantum kernel method via support vector machine has emerged as a powerful approach, drawing attention from various research groups [4, 5, 7, 13, 14, 16, 21, 22, 24, 25, 27, 29, 31, 32, 46]. In [14], two effective approaches were introduced for the construction of quantum SVMs: the Quantum Kernel Estimator and the Quantum Variational Classifier. These methods harness classical data and map it into the quantum state space via a quantum feature map. A pivotal element in this procedure is the quantum circuit, which facilitates the transformation of the dataset from its initial low-dimensional real space to a higher-dimensional quantum state space, commonly referred to as the Hilbert space

The choice of an appropriate feature map, matched to a suitable kernel, emerges as a decisive factor in the success of kernel methods. The selection of the right feature map becomes particularly critical depending on the dataset under consideration. [3] first proposed the genetic algorithm for the auto generation of feature map in quantum support vector machine. Additional advancements [8–11] have introduced the automatic generation of quantum feature maps

* haiyan.wang@asu.edu

through the utilization of multi-objective genetic algorithms. These algorithms provide a potent avenue for optimizing gate or circuit structures, circumventing common challenges like local minima and barren plateaus [34–36].

In previous works [3, 11], the design of feature maps have predominantly led to a suppression of entanglement gates. The benefit for less entanglement gates could reduce circuit numbers. However, entanglement, a fundamental concept in quantum mechanics, plays a pivotal role in enabling quantum computing and understanding its mathematical formulation is crucial. In this paper, we present several fitness functions for a multi-objective genetic algorithm that simultaneously maximizes classification accuracy while minimizing both the local and non-local gate costs of the quantum feature map’s circuit. Unlike the methods in [3, 11], we separate the optimization functions for local gates and non-local (controlled-NOT (CNOT)) gates. By doing so, we obtain a set of non-dominated points that reveal a more balanced configuration of quantum circuits for the quantum kernel method, incorporating a proportional number of CNOT gates to facilitate entanglement. Further analysis of this three-dimensional set of non-dominated points offers deeper insights into the feature map design.

The results of this paper indicate that various separability indexes can be used to help assessing the construct efficient quantum circuits for achieving high accuracy. Currently, the documentations for quantum kernels at <https://qiskit.org/> do not provide a guide for how these parameters should be chosen. For example, the entanglement parameter of ZZFeatureMap has three options: linear, full and circular. The results of this paper can be used to help choosing these parameters based on analysis of data.

Key new contributions of this paper are 1) designing three fitness functions for a genetic algorithms to demonstrate that the entanglement gates are needed to achieve high prediction accuracy, which improves/complements the result in [3, 11]. 2) experimentally demonstrate that the correlation between separability indexes of data and the number of entanglement gates, which provides a useful guide for the use of the relevant packages in <https://qiskit.org/> [2].

2. SUPPORT VECTOR MACHINE WITH QUANTUM KERNELS

2.1. Support vector machine

Support vector machines (SVMs) are a supervised learning method used for classification and regression. The goal is to find the optimal hyperplane that separates two classes by maximizing the margin. Mathematically, for a given labeled training set (x_i, y_i) where x_i are the features and y_i are the labels (+1 or -1), the optimization problem is:

$$\text{minimize } ||w||^2 \quad \text{subject to } y_i(w \cdot x_i + b) \geq 1, \quad \forall i$$

where w is the normal vector to the hyperplane, b is the bias term, and the constraints ensure we maximize the margin. This optimization finds the maximum margin hyperplane. The x_i points nearest the hyperplane are called support vectors. Overall, SVMs are powerful for complex classification and regression tasks.

This finds the maximum margin hyperplane. The x_i points nearest the hyperplane are called support vectors. To handle non-linear problems, SVMs use kernel functions to map the data to a higher dimensional space where separation is possible. Overall, SVMs are powerful for complex classification and regression tasks. The primal optimization problem can be alternatively represented as the Lagrange dual problem:

$$\begin{aligned}
\max \quad & L(w, b, \alpha) = \sum_{i=1}^n \alpha_i - \frac{1}{2} \sum_{i=1}^n \sum_{j=1}^n \alpha_i \alpha_j y_i y_j x_i x_j \\
\text{s.t.} \quad & \sum_{i=1}^n \alpha_i y_i = 0, \quad \alpha_i \geq 0
\end{aligned} \tag{1}$$

Kernel methods encompass a collection of pattern analysis algorithms that rely on the utilization of kernel functions, functioning within high-dimensional feature spaces. Among these, Support Vector Machines (SVMs) stand out as prominent supervised learning algorithms, especially tailored for classification tasks. The kernel function operates by implicitly mapping input data into these higher-dimensional spaces, thereby simplifying the problem-solving process. In essence, kernels possess the ability to transform originally non-linearly separable data distributions into linearly separable ones, a phenomenon commonly referred to as the "kernel trick."

The kernel function, denoted as $K(x_i, x_j) = \phi(x_i)^T \phi(x_j)$, enables SVM computations by only requiring knowledge of how to compute the inner product of $\phi(x_i)$ and $\phi(x_j)$, rather than explicit knowledge of the feature map ϕ . With the application of the kernel trick, we can reformulate the Lagrange dual problem as follows:

$$\begin{aligned}
\max \quad & L(w, b, \alpha) = \sum_{i=1}^n \alpha_i - \frac{1}{2} \sum_{i=1}^n \sum_{j=1}^n \alpha_i \alpha_j y_i y_j K(x_i, x_j) \\
\text{s.t.} \quad & \sum_{i=1}^n \alpha_i y_i = 0, \quad \alpha_i \geq 0
\end{aligned} \tag{2}$$

2.2. Quantum kernel method

In the context of quantum computing, the Quantum Kernel Estimator detailed in [14] presents effective strategies for crafting a quantum SVM and, specifically, the Quantum Variational Classifier. [14] achieves this by encoding data within the quantum state space through a quantum feature map. The choice of the feature map is a pivotal decision, often contingent on the characteristics of the dataset to be classified. It is worth noting that the feature map's significance extends beyond utilizing quantum state space as a feature space; it also involves the manner in which data is mapped into this high-dimensional space.

A significant challenge in quantum machine learning lies in the effective encoding of classical information into quantum states for quantum computing. The kernel method can be seamlessly integrated into quantum computing by conceptualizing the quantum circuit as an encoding function denoted as Φ , where the quantum feature map takes the form $|\Phi(x)\rangle = U(x)|0^n\rangle$. This naturally leads to the definition of the kernel as $K(x_i, x_j) = |\langle\Phi(x_i)|\Phi(x_j)\rangle|^2$. This approach facilitates the mapping of data points into the quantum Hilbert space [30], thereby leveraging the substantial advantages of quantum computing.

Through the utilization of quantum circuits, a data point $x \in \mathbb{R}^n$ is transformed into an n-qubit quantum feature state, $\Phi(x) = U(x)|0^n\rangle\langle 0^n|U^\dagger(x)$, achieved via a unitary circuit $U(x)$. This circuit serves as a powerful tool for evaluating the kernel as follows:

$$K(x_i, x_j) = |\langle\Phi(x_i)|\Phi(x_j)\rangle|^2 = |\langle 0^n|U^\dagger(x_i)U(x_j)|0^n\rangle|^2 \tag{3}$$

The quantum kernel estimation process entails evolving the initial state $|0^n\rangle$ on a quantum computer using $U^\dagger(x_i)U(x_j)$ and subsequently measuring the frequency of the outcome 0^n . As long as the computation of the quantum kernel $K(x_i, x_j)$ remains efficient, we can conduct optimization tasks within the Hilbert space, with other optimization steps executed on a classical computer. For a more in-depth understanding of quantum kernel estimation, please consult the detailed information provided in [14].

Developing feature maps based on quantum circuits that defy classical simulation is a crucial stride towards achieving a quantum advantage over classical methodologies. In this context, the work presented in [14] introduces a family of feature maps, conjectured to be classically hard to simulate, while being amenable to implementation as short-depth circuits on near-term quantum hardware. However, certain applications may warrant consideration of a more generalized form for the feature map.

In [14], various widely-recognized feature maps like ZFeatureMap and ZZFeatureMap are proposed. One approach to customization involves employing a Pauli feature map and specifying a set of Pauli gates, deviating from the default Z gates. In this paper, our objective is to tailor a feature map that shares common parameters with ZFeatureMap and ZZFeatureMap, such as 'reps' and the data map function, while introducing an additional parameter for Pauli gates to modify the gate set. This customized feature map will encompass ZFeatureMap and ZZFeatureMap as specific instances. For example, a representative form of our tailored quantum feature map might take the following structure:

$$\mathcal{U}_{\Phi(\mathbf{x})} = \left(\exp \left(i \sum_{j,k} \phi_{\{j,k\}}(\mathbf{x}) Z_j \otimes Z_k \right) \exp \left(i \sum_j \phi_{\{j\}}(\mathbf{x}) P_j \right) H^{\otimes n} \right)^d$$

where P_j can be one of the rotation gates X, Y, Z . The depth $d = 1$ version of this quantum circuit is shown in Figure 1 below for $n = 2$ qubits.

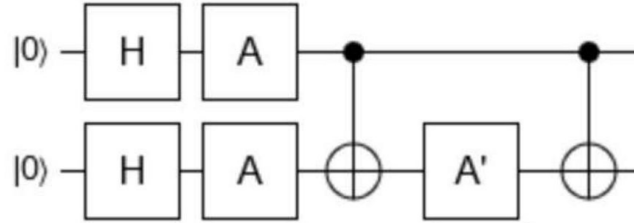


FIG. 1: Quantum circuit for $n = 2$ qubits

The circuit involves a layer of Hadamard gates $H^{\otimes n}$, followed by a subsequent layer of single-qubit gates $A = e^{i\phi_j(\mathbf{x})P_j}$. These A gates are characterized by a set of angles $\phi_j(\mathbf{x})$, each associated with a distinct axis, and $\phi_j(\mathbf{x})$ is contingent on the feature data. The diagonal entangling gate $e^{i\phi_{\{0,1\}}(\mathbf{x})Z_0 \otimes Z_1}$ is parametrized by an angle $\phi_{\{0,1\}}(\mathbf{x})$ and can be implemented using two CNOT gates and one $A' = e^{i\phi_{\{0,1\}}(\mathbf{x})Z_1}$ gate as shown in Figure 1.

Designing an appropriate kernel function for diverse datasets presents a formidable challenge. In our research, we employ a genetic algorithm to implement a global optimization approach for refining the structure of the quantum circuit. This methodology has proven to be effective in overcoming typical obstacles, such as barren plateaus, often encountered in conventional optimization techniques. As a result, it yields high-quality learning kernels [3, 12].

3. EVOLUTIONARY MULTI-OBJECTIVE OPTIMIZATION

Genetic algorithms belong to a formidable category of optimization methodologies that draw inspiration from the mechanisms of evolution. These algorithms traverse a solution space by iteratively refining a population of individuals, with each individual encoding a feature map. Over successive generations, genetic operations dictate the choice of offspring aimed at enhancing one or more objectives. This evolutionary dynamic effectively culminates in the selection of highly suitable individuals from within a vast configuration space.

The effectiveness and applicability of a genetic algorithm hinge significantly on the choice of genetic operations. Among these, the selection operator assumes a pivotal role as it determines a subset of the existing population to form a new generation through crossover and mutation operations. Mutation introduces random alterations to selected individuals' information, facilitating exploration of distant regions within the solution space. In contrast, crossover enables more radical exploration by exchanging genetic information between two individuals. Notably, mutation and crossover probabilities are fixed values, fine-tuned for optimal performance, while the selection probability is directly proportional to individuals' fitness.

To ensure the genetic algorithm's efficiency and convergence, early stopping conditions are employed to assess whether the evolutionary process has achieved its objectives. These conditions may involve monitoring the convergence or saturation of the fitness objective, maintaining a minimum accuracy threshold to continue the process, or setting a maximum number of generations. By leveraging these essential components, genetic algorithms emerge as valuable tools for addressing intricate optimization tasks across various domains.

An Evolutionary Multi-Objective Optimization (EMO) problem entails multiple objective functions that are subject to either minimization or maximization. Similar to single-objective optimization problems, multi-objective optimization problems may also incorporate various constraints that must be adhered to by all feasible solutions, including the optimal ones. For further insights, refer to [1, 6, 23].

In the realm of multi-objective optimization, optimal solutions are characterized by a mathematical concept known as partial ordering, and this concept is described using the term "domination." In this paper, our focus is primarily on addressing unconstrained optimization problems, which are devoid of any equality, inequality, or bound constraints. The notion of domination between two solutions is articulated as follows: Solution $\mathbf{x}^{(1)}$ is deemed to dominate another solution, $\mathbf{x}^{(2)}$, only if both of the following conditions hold true:

1. The solution $\mathbf{x}^{(1)}$ is no worse than $\mathbf{x}^{(2)}$ in all objectives. Consequently, the comparison between these solutions is made by evaluating their objective function values or by examining the positions of the corresponding points ($\mathbf{z}^{(1)}$ and $\mathbf{z}^{(2)}$) within the objective space.
2. The solution $\mathbf{x}^{(1)}$ is strictly better than $\mathbf{x}^{(2)}$ in at least one objective.

Points that remain not dominated by any other members within a set are termed as non-dominated points of class one, or simply non-dominated points. One distinctive feature of any two such points is that improvements in one objective only occur at the expense of at least one other objective—a trade-off relationship. This trade-off property among non-dominated points piques the interest of practitioners, as it encourages the exploration of a diverse array of such points before reaching a final decision. When these points are collectively considered in the objective space, they form a front, often referred to as a non-domination front.

If the set of points contains all possible points within the search space (assuming a countable number), the points residing on the non-domination front, by definition, are impervious to domination by any other point within the objective space. Consequently, they represent the Pareto-optimal points, collectively constituting the Pareto-optimal front. The Non-dominated Sorting Genetic Algorithm (NSGA-II) was initially designed to tackle various constrained problems, including a challenging five-objective seven-constraint nonlinear problem. NSGA-II, as outlined by Deb in 2002 [6], stands as one of the widely adopted Evolutionary Multi-Objective Optimization (EMO) techniques, geared towards identifying multiple Pareto-optimal solutions in multi-objective optimization scenarios. NSGA-II was developed as an evolutionary algorithm in response to the limitations of early evolutionary algorithms, which lacked elitism and employed a sharing parameter to maintain diversity within the Pareto set.

The resulting Pareto fronts for quantum feature maps serve as clear visual representations of the methodology for achieving high accuracy while keeping gate costs minimal. These Pareto-optimal fronts provide a meticulous means to analyze cost-effective trade-off strategies, especially in cases where numerous objectives might conflict with one another. Further examination of the three-dimensional Pareto-optimal fronts and their projections onto two-dimensional spaces offers deeper insights into the significant influence of entanglements on quantum kernel accuracy.

4. QUANTUM KERNEL FOR SUPPORT VECTOR MACHINE

4.1. Genetic quantum feature map

Based on the method in [3] for a multi-objective optimization process to generate quantum feature maps, here in this paper, we choose to implement the NSGA-II algorithm, which autonomously crafts and fine-tunes quantum classifiers using quantum feature maps and support vector machines. As we discuss before, the NSGA-II algorithm uses elitism and employs a sharing parameter to maintain diversity within the Pareto set. This algorithm delves into a parameterized quantum circuit's configuration space, potentially representing feature maps. It actively seeks out circuits that, once trained through machine learning methods, maximize accuracy when generalizing to the validation dataset, all while striving to minimize circuit complexity. This complexity is gauged in terms of local gates (including Hadamard gates and rotation gates) and CNOT gates. The algorithm's selection process for individuals advancing to the next generation hinges on Pareto-dominance and density-based metrics. For more comprehensive insights, please refer to [3, 6, 8, 11].

In the previous studies [3, 11], it is found that the number of entanglement gates are sacrificed by the local gates for reducing the number of circuits. In this paper, we separate CNOT gates from local gates and add two optimizing functions. We modified the encoding method [3, 11] to create a quantum circuit with a minimum of local and CNOT gates and maximum of accuracy. To simplify the problem, we choose the feature number as the number of qubits (N). Our encoding scheme begins with N number H gates and N possible rotation gates and extra two bits to indicate a rotation with respect to X, Y, Z , followed by possible H entanglement which can be implemented by two rotation gates and a CNOT gates as shown in Figure 1, the last two bits are reserved for repetitions. We also include the data into the encoding. Because the feature number is the same as the number of qubits, thus the i -th gene that operates on the qubits of the quantum register possibly depends on the i -th variable from the input data $\mathbf{x} \in \mathbb{N}^d$. Specifically, rotation gate is parameterized by a value in the input data.

$$R_\alpha(x_k) = \exp(-i \frac{x_k}{2} \sigma^\alpha)$$

where σ^α are one of Paulis $= [X, Y, Z]$. As we see from Figure 1, an entanglement between circuits i, j can be implemented using two CNOT gates and rotation $e^{i\phi_{\{0,1\}}(x)Z_1}$ gate. For the rotation gate of the entanglement implementation between circuits i, j . The rotation parameter is chosen to be $x_i x_j$ as $R_Z(x_i x_j) = \exp(-i \frac{x_i x_j}{2} Z)$.

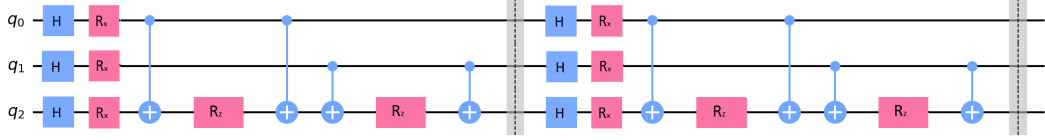


FIG. 2: Example for encoding scheme: the number of qubits is 3, the binary bits are $[1, 1, 1, 1, 0, 0, 1, 1, 1, 0]$, the first three bits for 3 rotation gates, and next two bits indicates the rotation with respect to X, Y, Z , followed 3 bits for possible entanglements, the last two bits is for repetitions.

To illustrate the comprehensive encoding scheme encompassing various types of gates, we employ three qubits and allocate 10 bits per gene, as depicted in Figure 2. The genetic algorithm involves an initial population of individuals, represented by bit strings with a size of $N + \binom{N}{2} + 4$. The evaluation function deciphers each individual, constructing an associated quantum circuit. This circuit, in conjunction with the training dataset, is employed to assess the corresponding kernel matrices, which are then integrated into SVM algorithms for fitness function computation. Individuals exhibiting superior fitness are more likely to be selected and subjected to diverse genetic operations, including mutation, crossover, and selection, resulting in the creation of a new generation of individuals or quantum circuits. This iterative process continues until the convergence criteria are met.

4.2. Fitness functions

Fitness, in this context, serves as the objective function or cost function. It takes a solution as input and yields the fitness score for that solution. Based on the fitness functions proposed in [3], we introduce three fitness functions below (4), our aim is twofold: to **maximize accuracy** and **minimize both of local and non-local gate costs**. In tackling multi-objective problems, a common strategy involves identifying the Pareto front [1, 6, 23], which entails selecting high-dominance points using crowd distance techniques. Recognizing that different gates may entail distinct costs [3, 11, 20], we distinguish CNOT gates from local gates and introduce two fitness optimization functions. The resulting three-dimensional Pareto fronts offer valuable insights for devising cost-effective trade-off strategies. Accuracy, in this context, denotes the mean accuracy achieved on the provided test data and labels, using the SVM model generated by a quantum circuit. Gate costs are computed by counting the sequence of basic physical operations required for quantum computer implementation.

$$\begin{cases} (\text{maximize}) \text{Fitness 1} = \text{prediction accuracy} \\ (\text{minimize}) \text{Fitness 2} = \text{local gates} = \text{Rgate} + \text{Hgate} \\ (\text{minimize}) \text{Fitness 2} = \text{CNOT gate} \end{cases} \quad (4)$$

Our fitness function is crafted to optimize two key aspects: the maximization of classification accuracy and the minimization of the variational circuit’s complexity for both local and non-local gates. In the pursuit of this optimization, we undertake a rigorous evaluation process. This process entails dividing the dataset into distinct training and test sets. Utilizing the quantum circuit in tandem with the training set, we compute the classifier, employing the quantum kernel SVM. Subsequently, we gauge the model’s performance by assessing its accuracy over the test set.

The Pareto front, a crucial outcome of our genetic algorithm-driven process, plays a pivotal role in striking a delicate balance between these three critical performance metrics. In our pursuit of equilibrium, we deliberately choose not to introduce weights to the objective functions. Such weighting could exert undue influence on both accuracy and gate count, potentially skewing the optimization process.

5. EXPERIMENTS WITH TWO DATASETS

Based on the method in [3] for a multi-objective optimization process to generate quantum feature maps, we employ high-dimensional NSGA-II in conjunction with quantum kernels on two datasets: one is the breast cancer dataset containing 30 features, and the other is the Iris dataset with 4 features. To intensify the challenge for achieving high accuracy, we deliberately opt not to employ principal component analysis (PCA) for dimension reduction. [3] details the training algorithm iterated until convergence is reached. We choose an initial random population of individuals represented as binary chains, each comprising $N + \binom{N}{2} + 4$ bits, where N represents the maximum number of qubits. Once each individual is decoded and transformed into a quantum circuit, we proceed to genetic algorithm operators such as selection, crossover, and mutation to generate the next generation of individuals. Then we compute the kernel of a quantum SVM while training a classifier with the provided training dataset. In each loop, we evaluate the accuracy of the classifier using the test dataset and assess the effective size of the circuit in terms of the number of local and entangling gates it contains.

5.1. Breast cancer dataset

We initiate our analysis with the breast cancer dataset, sourced from Sklearn [26, 77]. This dataset contains measurements of breast tissue derived from a medical imaging technique, including various measurements related to cell nuclei. The primary objective is to ascertain whether a tumor is benign (harmless) or malignant (cancerous and dangerous).

The breast cancer dataset, imported from scikit-learn, comprises 569 samples, encompassing 30 real, positive features. These features encompass attributes related to cancer mass, such as mean radius, mean texture, mean perimeter, and more. Among these samples, 212 are labeled as "malignant," while 357 are labeled as "benign."

To facilitate our analysis, we organize this data into a feature matrix of dimensions 569 by 30 and a target vector of dimension 569. Subsequently, we randomly select a number of features equal to the number of quantum circuits and allocate 100 rows for training and 50 rows for testing purposes.

Having our training and testing datasets prepared, we proceed with the previously outlined procedure to compute the training and testing quantum kernel matrices. These quantum kernels can subsequently be integrated into classical kernel methods.

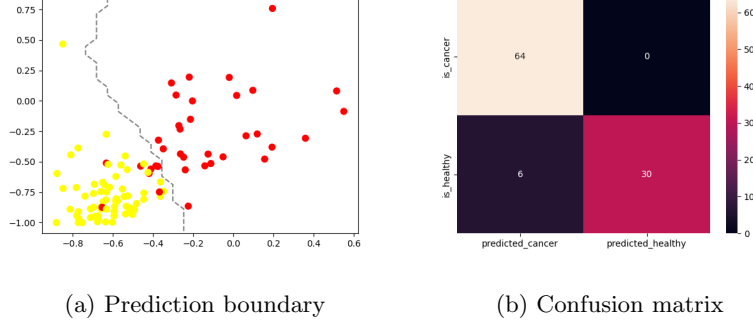


FIG. 3: Prediction boundary and confusion matrix

Figure 3a illustrates the data points and prediction boundaries resulting from the quantum kernel SVM in a two-qubit scenario, while Figure 3b presents the corresponding confusion matrix. The confusion matrix is a pivotal tool for evaluating the performance of a classification algorithm. Together, these elements furnish an estimate of the quantum kernel matrix, which can be harnessed as a kernel for support vector classification.

We conducted a comprehensive comparison of various kernels and quantum feature mapping techniques. Specifically, we assessed the performance of four well-established classical kernels ('Linear,' 'Poly,' 'RBF,' 'Sigmoid'). To ensure robustness in our analysis, we randomly selected 50 feature combinations for each qubit size. The results, summarized in Table 1 and illustrated in Figure 4, showcase the average best accuracy achieved by each prediction method across different feature and qubit configurations.

Our findings reveal that, in comparison to classical kernel methods, the quantum kernel generated by the genetic algorithm consistently outperforms all classical kernels with the dataset. Notably, the RBF kernel exhibits superior performance among the classical kernels. These results underscore the suitability of the quantum kernel for the given dataset, highlighting its potential as a powerful tool for enhancing classification tasks.

TABLE 1: Accuracy comparison for kernel methods with breast cancer dataset. The accuracy is calculated as the average of the best accuracies for the 50 randomly selected features.

Kernel Method	Number of features/qubits								
	2	3	4	5	6	7	8	9	10
Linear	0.82	0.86	0.9	0.91	0.93	0.93	0.93	0.94	0.95
Poly	0.83	0.88	0.9	0.91	0.93	0.93	0.93	0.94	0.94
RBF	0.84	0.88	0.9	0.91	0.93	0.93	0.93	0.93	0.94
Sigmoid	0.74	0.75	0.78	0.95	0.82	0.81	0.8	0.82	0.82
Quantum	0.85	0.90	0.93	0.95	0.96	0.96	0.96	0.97	0.97

Furthermore, Table 2 and Figure 5 provide valuable insights into the average quantities of local and CNOT gates associated with our quantum circuits. It's noteworthy that in our experiments with the dataset, we observe a reasonable proportionality between the number of CNOT gates and the number of local gates. This finding deviates from the observations made in [3, 11], where entanglement gates were predominantly suppressed.

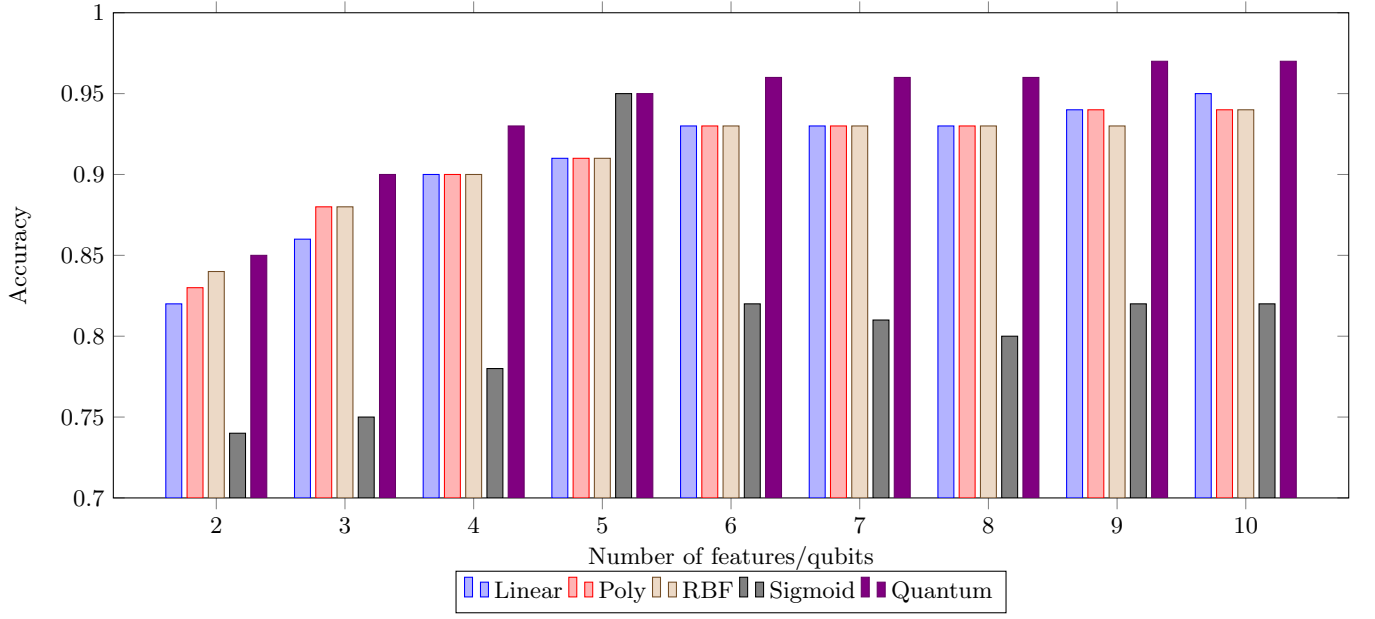


FIG. 4: Accuracy comparison for kernel methods with breast cancer dataset

TABLE 2: Gate numbers of Quantum feature map with breast cancer data. The gate numbers are calculated as the average gates with the best accuracies of the 50 randomly selected features.

Gate	Number of features/qubits								
	2	3	4	5	6	7	8	9	10
Local gates	11.42	14.98	17.4	24.52	21.46	29.2	31.84	37.18	40.12
CNOT gates	2.48	5.96	10.4	17.36	18.0	26.68	32.16	40.2	45.64

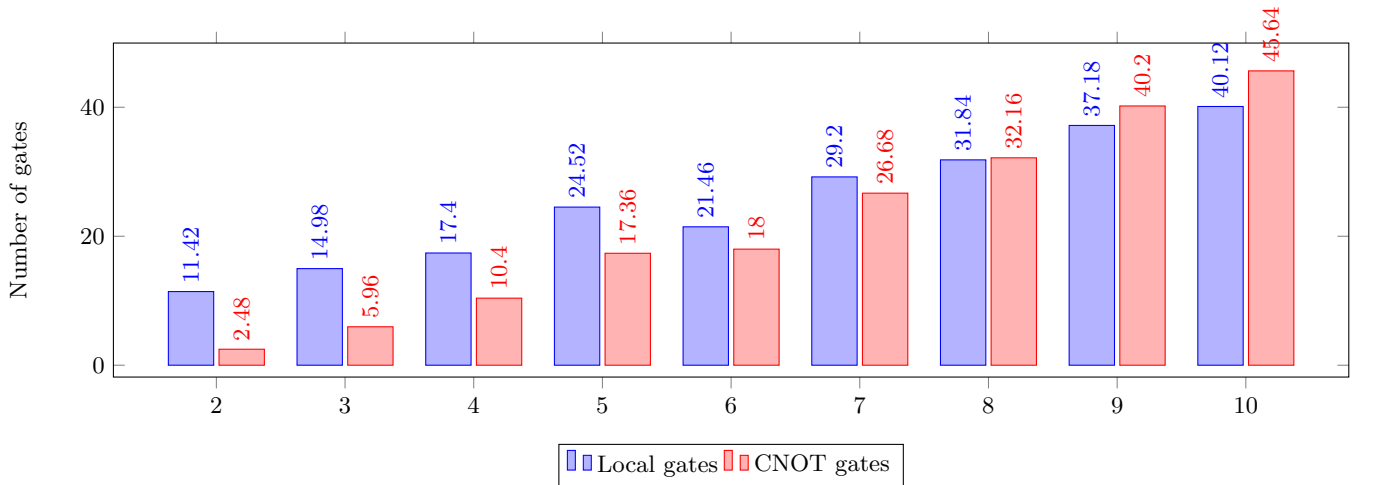


FIG. 5: Gate numbers of Quantum feature map with breast cancer data.

The discrepancy may be attributed to the optimization functions employed in [3], which introduce weighting factors to strike a balance between the relative significance of the two performance metrics. As detailed in [3], assigning a high weight to accuracy can lead to a convergence into a single individual, thereby eroding the necessary genetic diversity crucial for minimizing the quantum circuit’s size throughout evolution. Conversely, an excessively low gate count can impede the quantum kernel’s ability to effectively discern features.

5.2. Iris dataset

TABLE 3: Accuracy comparison for the kernel methods with Iris dataset. The best accuracy for each prediction method with the different features

Kernel Method	Number of features/qubits		
	2	3	4
Linear	0.96	0.99	1
Poly	0.96	0.99	1
RBF	0.95	0.99	1
Sigmoid	0.88	0.94	0.95
Quantum	0.96	0.99	1

TABLE 4: Gate numbers for the quantum kernel method with Iris data. Gate numbers with the best accuracy

Gate	Number of features/qubits		
	2	3	4
Local gates	3.17	4	5
CNOT gates	0	0	0

Next, our attention turns to the Iris dataset, which encompasses data on three distinct types of irises: Setosa, Versicolour, and Virginica. This dataset includes measurements of petal and sepal length, organized in a 150x4 array format, where the rows represent individual samples, and the columns encompass Sepal Length, Sepal Width, Petal Length, and Petal Width.

Given the dataset’s relatively limited feature set of only 4 features, and in a deliberate departure from random feature selection, we opt to evaluate the performance with 2, 3, and 4 features individually. In fact, this equates to a total of 6 features when using 2 qubits, 4 features with 3 qubits, and a single feature represented by 4 qubits. Subsequently, we execute a consistent procedure, gauging accuracy and facilitating a comparative analysis between quantum kernels and classical SVM kernels.

We employ the same procedure as applied to the breast cancer dataset to perform a comparative analysis of various kernels, including those generated from quantum feature maps. Table 3 showcases the highest accuracy achieved by each prediction method across varying numbers of features or qubits.

When assessing the classical kernel methods, it becomes evident that the quantum kernel generated by a genetic algorithm either matches or surpasses the performance of classical kernels with this dataset. Table 4 provides insights into the corresponding counts of local and CNOT gates utilized within the quantum circuits. Notably, for the Iris dataset, it is observed that the majority of CNOT gates are zero. This phenomenon may be attributed to the effectiveness of local gates in achieving high accuracy, rendering the inclusion of entanglements unnecessary in this scenario.

5.3. Data separability and non-local gates

In this section, our objective is to look into the impact of data complexity, specifically, data separability, on the prevalence of entanglement circuits. In the realm of machine learning, the efficacy of a classifier is contingent on two critical factors: the classifier model itself and the degree of separability or complexity inherent in the datasets under consideration. This characterization of data complexity often takes into account various factors, such as the data distribution, as well as estimates of the shape and size of the decision boundary [19].

For the sake of comparison and a quantitative assessment of dataset separability, we have chosen three distinct indices as measures. These indices provide valuable insights into the separability of the datasets and are instrumental in our analysis.

The first index is the separability index (SI) measure which estimates the average number of instances in a dataset that have a nearest neighbor with the same label. Since this is a fraction, the index varies between 0-1 or 0-100%. Another separability measure, based on the class distance or margin is the hypothesis margin index (HMI), introduced in [18]. It measures the distance between an object's nearest neighbor of the same class (near-hit) and a nearest neighbor of the opposing class (near-miss) and sums over these.

$$\theta_P(x) = \frac{1}{2}(\|x - \text{nearmiss}(x)\| - \|x - \text{nearhit}(x)\|)$$

where $\text{nearhit}(x)$ and $\text{nearmiss}(x)$ denote the nearest point to x in P with the same and different label, respectively. Therefore, large hypothesis-margin ensures large sample-margin, and the dataset has high separability. Margins occupy a pivotal position in contemporary machine learning research, serving as essential metrics to gauge the classifier's confidence during decision-making. These margins serve a dual purpose: they are employed to establish theoretical generalization bounds and provide valuable insights for algorithm design. It is imperative to note that as the near-miss distance increases and near-hit values decrease, the hypothesis margin index proportionally expands.

The third index is the distance-based separability index (DSI) which was recently introduced in [17]. They identified scenarios where different data classes are blended within the same distribution as particularly challenging for classifiers to disentangle. Prior to introducing the DSI (Data Separability Index), we first introduce two fundamental components: the intra-class distance (ICD) and the between-class distance (BCD) sets. These components are instrumental in the computation of the DSI. Suppose X and Y have N_x and N_y data points, respectively. The intra-class distance (ICD) set $\{d_x\}$ is a set of distances between any two points in the same class (X), as: $\{d_x\} = \{\|x_i - x_j\|_2 | x_i, x_j \in X; x_i \neq x_j\}$. The between-class distance (BCD) set $\{d_{x,y}\}$ is the set of distances between any two points from different classes (X and Y), as $\{d_{x,y}\} = \{\|x_i - y_j\|_2 | x_i \in X; y_j \in Y\}$. The metric for all distances is *Euclidean* (l^2 norm). We firstly introduce the computation of the DSI for a dataset containing only two classes X

and Y . First, the ICD sets of X and Y : $\{d_x\}, \{d_y\}$ and the BCD set: $\{d_{x,y}\}$ are computed by their definitions. The similarities between the ICD and BCD sets are then computed using the Kolmogorov–Smirnov (KS) distance

$$s_x = KS(\{d_x\}, \{d_{x,y}\}), \text{ and } s_y = KS(\{d_y\}, \{d_{x,y}\}).$$

Finally, the DSI is the average of the two KS distances:

$$DSI(\{X, Y\}) = \frac{(s_x + s_y)}{2}.$$

TABLE 5: Separability indexes of breast cancer data

Separability Index	Number of features/qubits								
	2	3	4	5	6	7	8	9	10
SI	0.78	0.82	0.84	0.87	0.88	0.88	0.88	0.89	0.90
HMI	4.18	5.82	7.47	8.53	10.82	10.75	11.61	12.46	13.36
DSI	0.27	0.28	0.32	0.34	0.38	0.35	0.35	0.36	0.37

TABLE 6: Separability indexes of Iris data

Separability Index	Number of features/qubits		
	2	3	4
SI	0.9	0.94	0.95
HMI	8.29	10.46	12.19
DSI	0.78	0.80	0.82

For the breast cancer dataset, for each qubit size, we randomly select 50 combinations of the features with this size, Table 5 presents the corresponding average numbers of the three separability indexes along with each number of the features/qubits. For comparison, we calculated the corresponding average three separability indexes for three qubits/features in Table 6 for the Iris dataset (in fact, there are only 6 features with 2 qubits, and 4 features with 3 qubits and one feature with 4 qubits). This comparison of the separability indexes for the two datasets may explain why we need more CNOT gates for the breast cancer dataset. From the definitions, it is clear that *the higher the three indexes are, the easier it is to separate a dataset*. Clearly the separability indexes for the Iris dataset are larger than those of the breast cancer dataset, which explains why the quantum feature maps for the breast cancer dataset needs more CNOT gates to achieve high accuracy. For the Iris data, which has much higher separability indexes, and it seems that the CNOT gates are almost zero. In addition, for the breast cancer dataset, we see that the higher dimensions of features/qubits, the more CNOT gates are needed. This indicates that entanglements may be only needed for lower separability indexes and high dimensional qubits.

6. CONCLUSION AND DISCUSSION

In this study, based on the method in [3], we present a several fitness functions for a multi-objective genetic algorithm, specifically NSGA-II, to design quantum kernel feature maps for support vector machines. Our approach

optimizes the quantum feature map of quantum kernels through the genetic algorithm and demonstrates that the need of entanglement gates for high accuracy. Notably, we segment the optimization functions into two categories: one for local gates and the other for non-local gates (CNOT gates). The experimental results in this work shed light on the composition of quantum kernel maps for support vector machines, indicating a proportional inclusion of CNOT gates for entanglement. This observation stands in contrast to prior findings in [3, 11], where CNOT gates were significantly suppressed.

Entanglement, a central concept in quantum mechanics, plays a pivotal role in enabling quantum computing and is integral to our understanding of its mathematical formulation. Further analysis of the three-dimensional set of non-dominated points provides deeper insights into feature map design. Our experiments also suggest that higher-dimensional qubits may necessitate a greater number of CNOT gates to achieve high prediction accuracy.

This study employs three separability indexes to investigate the impact of data on the configuration of feature maps in quantum support vector machines. Our experiments reveal that, for the same dataset, higher-dimensional qubits may require an increased number of CNOT gates to achieve improved prediction accuracy. Moreover, datasets with less separability indexes tend to benefit from additional CNOT gates to attain high prediction accuracy. These findings highlight the utility of various separability indexes in aiding the design of efficient quantum circuits for achieving heightened accuracy.

It’s noteworthy that the current documentation for quantum kernels on <https://qiskit.org/> lacks guidance on parameter selection. For instance, the entanglement parameter in ZZFeatureMap offers three options: linear, full, and circular. The insights from this paper can serve as a valuable resource for making informed decisions regarding these parameters based on data analysis.

The analysis of data separability reveals an interesting trend: less data separability necessitates the utilization of more CNOT gates to achieve accurate predictions. This observation is poised to inform the design of more efficient quantum circuits for machine learning applications. Future research endeavors could focus on refining indexes and metrics for assessing data separability, potentially unveiling the presence of a quantum advantage more effectively.

The integration of quantum computing with machine learning presents an exciting frontier, with potential to transform the landscape of computation and expand the horizons of problem-solving across various domains. The potential advantages of using quantum kernel estimation to enhance machine learning applications are still being explored [46]. Leveraging qubit entanglement, quantum computers exhibit the capability to execute optimization and machine learning tasks at significantly accelerated speeds compared to classical computers. To evaluate the potential quantum advantage in learning tasks, [16] and [7] have introduced various metrics based on the geometric difference of data in relation to feature spaces. It’s important to note that there is no universally superior model in machine learning; the effectiveness of a model depends on the distribution of training data. [16] have developed a methodology for assessing potential quantum advantages in learning tasks, with the geometric difference of data serving as an initial measure to evaluate quantum kernels. This metric is associated with feature spaces and provides insight into the differences in prediction errors between two scrutinized kernels [7].

The Pareto fronts generated from several fitness functions for genetic algorithms illustrate the methodology for attaining high accuracy while concurrently minimizing gate costs and other associated properties. These Pareto-optimal fronts afford us the opportunity to examine cost-effective trade-off strategies, particularly in scenarios where multiple objectives may be in conflict with each other. An exploration of the three-dimensional Pareto-optimal fronts and their projections onto two-dimensional spaces furnishes additional insights into the substantial influence of

entanglements on quantum kernel accuracy.

7. ACKNOWLEDGEMENT

The author would like to thank Allison Brayro and Nao Yamamoto for their reading and comments. Professors Sergio Altares-López, Juan José García-Ripoll, Angela Ribeiro have read the previous versions of this paper and provide constructive comments.

-
- [1] E.B. Alaia, I.H. Dridi, H. Bouchriha and P. Borne, *Genetic algorithm with pareto front selection for multi-criteria optimization of multi-depots and multi- vehicle pickup and delivery problems with time windows*, 2014 15th International Conference on Sciences and Techniques of Automatic Control and Computer Engineering, pp. 488-493, (2014).
 - [2] G. Aleksandrowicz et al, *Qiskit: An Open-source Framework for Quantum Computing*, Zenodo, (2019).
 - [3] S. Altares-López, A. Ribeiro, J.J. García-Ripoll, *Automatic design of quantum feature maps*, Quantum Science and Technology, vol. 6, no. 4, (2021).
 - [4] J. Biamonte, P. Wittek, N. Pancotti, P. Rebentrost, N. Wiebe and S. Lloyd, *Quantum machine learning*, Nature 549, pp. 195-202, (2017).
 - [5] A. Baughman, K. Yogaraj, R. Hebbar, S. Ghosh, R.U. Haq and Y. Chhabra, *Study of Feature Importance for Quantum Machine Learning Models*, arXiv:2202.11204, (2022).
 - [6] K. Deb, S. Agrawal, A. Pratap, T. Meyarivan, *A fast and Elitist multi-objective Genetic Algorithm: NSGA-II.*, IEEE Transactions on Evolutionary Computation. 2002;6(2):182-197.
 - [7] Di Marcantonio, Francesco and Incudini, Massimiliano and Tezza, Davide and Grossi, Michele, *Quantum Advantage Seeker with Kernels (QuASK): a software framework to speed up the research in quantum machine learning*, Quantum Machine Intelligence 5 (1), 2023
 - [8] B. Barán, A. Carballude and M. Villagra *Neighbor Optimization of N-Dimensional Quantum Circuits*, SN Computer Science 2, 2021
 - [9] D. Chivilikhin, A. Samarin, V. Ulyantsev, I. Iorsh, A.R. Oganov and O. Kyriienko, *MoG-VQE: Multiobjective genetic variational quantum eigensolver*, arXiv:2007.04424, (2020).
 - [10] P. Chen, L. Yuan, Y. He and S. Luo, *An improved SVM classifier based on double chains quantum genetic algorithm and its application in analogue circuit diagnosis*, Neurocomputing, vol. 211, pp. 202-211, (2016).
 - [11] B.-S. Chen, J.-L. Chern, *Generating quantum feature maps for SVM classifier*, arXiv:2207.11449, (2022).
 - [12] M. Gönen and E. Alpaydin, *Multiple Kernel Learning Algorithms*, Journal of Machine Learning Research, vol. 12, pp. 2211-2268, (2011).
 - [13] J.R. Glick, T.P. Gujarati, A.D. Córcoles, Y. Kim, A. Kandala, J.M. Gambetta and K. Temme, *Covariant quantum kernels for data with group structure*, APS March Meeting 2022, vol. 67, no. 3, (2022).
 - [14] V. Havlíček, A.D. Córcoles, K. Temme, M. Takita, M. Kandala, J.M. Chow and J.M. Gambetta, *Supervised learning with quantum-enhanced feature spaces*, Nature 567, pp. 209-212, (2019).
 - [15] Du Y, Hsieh M H, Liu T and Tao D *Physical Review Research* **2** 2020 URL <https://doi.org/10.1103/physrevresearch.2.033125>
 - [16] Huang H-Y, Broughton M, Mohseni M, Babbush R, Boixo S, Neven H, McClean JR *Power of data in quantum machine learning*, Nature Communications (2021) 12(1). <https://doi.org/10.1038/s41467-021-22539-9>

- [17] S. Guan, M. Loew, *A novel intrinsic measure of data separability*, Appl Intell 52, 17734–17750 (2022). <https://doi.org/10.1007/s10489-022-03395-6>
- [18] R. Gilad-Bachrach, A. Navot, N. Tishby, *Margin based feature selection - theory and algorithms*, ICML '04: Proceedings of the twenty-first international conference on Machine learning, July 2004. <https://doi.org/10.1145/1015330.1015352>
- [19] Ana C. Lorena and Luís P. F. Garcia and Jens Lehmann and Marcilio C. P. Souto and Tin Kam Ho *How Complex Is Your Classification Problem?: A Survey on Measuring Classification Complexity* ACM Computing Surveys, 52(5), 2019, <https://doi.org/10.1145/3347711>,
- [20] S. Lee, S.J. Lee, T. Kim, J.S. Lee, J. Biamonte and M. Perkowski, *The cost of quantum gate primitives*, Journal of Multiple-Valued Logic and Soft Computing, vol. 12, No. 5-6. pp. 561-573, (2006).
- [21] Y. Liu, S. Arunachalam and K. Temme, *A rigorous and robust quantum speed-up in supervised machine learning*, Nature Physics, vol. 17, pp. 1013-1017, (2021).
- [22] M. Mafu and M. Senekane, *Design and Implementation of Efficient Quantum Support Vector Machine*, 2021 International Conference on Electrical, Computer and Energy Technologies, pp. 1-4, (2021).
- [23] K. Miettinen, *Nonlinear Multiobjective Optimization*, Boston: Kluwer; 1999.
- [24] S. Moradi, C. Brandner, C. Spielvogel, D. Krajnc, S. Hillmich, R. Wille, W. Drexler and L. Papp, *Clinical data classification with noisy intermediate scale quantum computers*, Scientific Reports, vol. 12, no. 1851, (2022).
- [25] J.E. Park, B. Quanz, S. Wood, H. Higgins and R. Harishankar, *Practical application improvement to Quantum SVM: theory to practice*, arXiv:2012.07725, (2020).
- [26] F. Pedregosa, G. Varoquaux and A. Gramfort et al, *Scikit-learn: Machine Learning in Python*, Journal of Machine Learning Research, vol. 12, pp. 2825-2830, (2011).
- [27] P. Rebentrost, M. Mohseni, and S. Lloyd, *Quantum Support Vector Machine for Big Data Classification*, Physical Review Letters 113, 130503, (2014).
- [28] M. Schuld, N. Killoran *Is quantum advantage the right goal for quantum machine learning?* PRX Quantum 3:030101. (2022) <https://doi.org/10.1103/PRXQuantum.3.030101>
- [29] M. Schuld, *Quantum machine learning models are kernel methods*, arXiv:2101.11020, (2021).
- [30] M. Schuld and N. Killoran, *Quantum Machine Learning in Feature Hilbert Spaces*, Physical Review Letters 122, 040504, (2019).
- [31] M. Schuld, I. Sinayskiy and F. Petruccione, *An introduction to quantum machine learning*, Contemporary Physics, vol. 56, (2015).
- [32] Y. Suzuki, H. Yano, Q. Gao, S. Uno, T. Tanaka, M. Akiyama and N. Yamamoto, *Analysis and synthesis of feature map for kernel-based quantum classifier*, Quantum Machine Intelligence, vol. 2, no. 9, (2020).
- [33] J. R. McClean, S. Boixo, V. N. Smelyanskiy, R. Babbush, and H. Neven *Barren plateaus in quantum neural network training landscapes* Nature Communications, 9 (2018), URL <https://doi.org/10.1038/s41467-018-07090-4>
- [34] R. Li, U. Alvarez-Rodriguez, L. Lamata, and E. Solano *Quantum Measurements and Quantum Metrology* 2017 4 1–7 ISSN 2299-114X
- [35] L. Lamata, U. Alvarez-Rodriguez, J. D. Martín-Guerrero, M. Sanz, and E. Solano 2018 *Quantum Science and Technology* 4 014007 ISSN 2058-9565 URL <http://dx.doi.org/10.1088/2058-9565/aae22b>
- [36] D. Chivilikhin, A. Samarin, V. Ulyantsev, I. Iorsh, A. R. Oganov, and O. Kyriienko 2020 *Mog-vqe: Multiobjective genetic variational quantum eigensolver (Preprint 2007.04424)*
- [37] G. Mengoni and A. Di Pierro, *Quantum feature maps with entangled states*, arXiv:1912.03674, (2019).
- [38] M. Schuld and I. Petruccione, *Quantum natural gradient*, Physical Review A, 103(3), 032630 (2021).
- [39] K. Mitarai, M. Negoro, M. Kitagawa, and K. Fujii, *Quantum circuit learning*, Physical Review A, 98(3), 032309 (2018).

- [40] A. Abbas, D. Sutter, C. Zoufal, A. Lucchi, A. Figalli, and S. Woerner, *The power of quantum neural networks*, *Nature Computational Science*, 1(6), 403-409 (2021).
- [41] J.R. McClean, S. Boixo, V.N. Smelyanskiy, R.B.abbasne, A.W. Harrow, I.L. Markov, and T. Monz, *Barren plateaus in quantum neural network training landscapes*, *Nature Communications*, 9(1), 4812 (2018).
- [42] Z. Holmes, R. Schmied, and P. F. O'Malley, *Breakdown of training in deep quantum learning*, *Quantum*, 5, 462 (2021).
- [43] Z. Wang, A. Chia, Z. Wang, Y. Gong, J. Roland, and S. Lloyd, *Training quantum circuits with projective measurement*, *arXiv:2106.11495*, (2021).
- [44] A. Arrasmith, M. Cerezo, P. Czarnik, L. Cincio, and P.J. Coles, *Effect of barren plateaus on gradient-free optimization*, *Quantum*, 5, 558 (2021).
- [45] Z. Holmes, K. Sharma, and P.F. O'Malley, *Expressibility and entangling capability of parameterized quantum circuits for hybrid quantum-classical algorithms*, *Physical Review Research*, 4(3), 033099 (2022).
- [46] M. Schuld and N. Killoran, *Quantum machine learning for the quantum class*, *arXiv:2201.01548*, (2022).
- [47] L. Liu and P. Rebentrost, *An adaptive quantum algorithm for linear systems of equations*, *arXiv:1811.05371*, (2018).
- [48] K. Bartkiewicz, G. Chimini, M. Cianciaruso, A. C. Bertrand, and D. Wisniewski, *Experimental realization of quantum kernels*, *Physical Review Letters*, 125(10), 100503 (2020).
- [49] A. Paszke, S. Gross, F. Massa, A. Lerer, J. Bradbury, G. Chanan, T. Killeen, Z. Lin, N. Gimelshein, L. Antiga, et al, *PyTorch: An imperative style, high-performance deep learning library*, *Advances in Neural Information Processing Systems*, 8024-8035 (2019).
- [50] F. Chollet et al, *Keras*, *GitHub*, <https://github.com/fchollet/keras>.
- [51] V. Bergholm, J. Izaac, M. Schuld, C. Gogolin, M. Broughton, and N. Killoran, *PennyLane: Automatic differentiation of hybrid quantum-classical computations*, *arXiv:1811.04968*, (2018).
- [52] A. Anis, T. Bromley, J. Broughton, J. Izaac, T. Killoran, C. Bergholm, N. Cottrell, S. Gidney, T. Gokyigit, S. Guha, et al, *Tensorflow quantum: A software framework for quantum machine learning*, *arXiv:2101.01178*, (2021).
- [53] M. Broughton, M. Schuld, T. Farrow, M. Benenti, and D. Egger, *High performance quantum circuit simulator for OpenQASM 3.0*, *arXiv:2012.09895*, (2020).
- [54] N. Killoran, J. Izaac, M. Quesada, and S. McArdle, *Strawberry fields: A software platform for photonic quantum computing*, *Quantum*, 3, 129 (2019).
- [55] Baidu Quantum Team, *Paddle quantum: A quantum machine learning framework*, *GitHub*, <https://github.com/PaddlePaddle/Quantum>.
- [56] M. Lipow, *A program development and maintenance costs taxonomy*, *Communications of the ACM*, 25(7), 462-464 (1982).
- [57] A. Trisovic, J. Tschopp, P. Robinson, A. Romoser, S. Scott, J. Mangelson, J. Martel, D. Rigby, E. Toczyski, D. Jensen, et al, *Reproducibility in machine learning for health care*, *arXiv:2212.00812*, (2022).
- [58] P. Mineault and T. Nozawa, *Designing reproducible computational workflows*, *arXiv:2110.08655*, (2021).
- [59] T. Botvinik-Nezer, F. Holzmeister, C.F. Camerer, A. Dreber, J. Huber, M. Johannesson, M. Kirchler, J. I. Krajbich, G. Poldrack, T. Schonberg, et al, *Variability in the analysis of a single neuroimaging dataset by many teams*, *Nature*, 582(7810), 84-88 (2020).
- [60] M. A. Campos and M. G. Souto, *The challenges of code maintenance and reuse in scientific research software*, *Journal of Systems and Software*, 172, 110793 (2021).
- [61] B. Schölkopf, R. Herbrich, and A.J. Smola, *A generalized representer theorem*, *In Conference on Learning Theory*, 416-426 (2001).
- [62] F. Pérez-Cruz and O. Bousquet, *Generalized kernel matrices*, *Advances in Neural Information Processing Systems*, 1041-1048 (2004).

- [63] J.L. Rojo-Álvarez, A. Muñoz, M. Maudes, and C. Jutten, *Functional component analysis for functional data*, *Chemometrics and Intelligent Laboratory Systems*, 176, 91-98 (2018).
- [64] G. Camps-Valls, *Kernel methods in hyperspectral image analysis*, *IEEE Signal Processing Magazine*, 23(2), 135-141 (2006).
- [65] A. Ben-Hur, D. Horn, H. Siegelmann, and V. Vapnik, *Support vector clustering*, *Journal of Machine Learning Research*, 2, 125-137 (2008).
- [66] Y. Wang and J. Qi, *Nonlinear manifold learning for image restoration*, *IEEE Transactions on Image Processing*, 23(7), 2946-2957 (2014).
- [67] J. Yang, *Kernel eigenfaces vs. kernel fisherfaces: Face recognition using kernel methods*, *Proceedings of the 2001 IEEE Computer Society Conference on Computer Vision and Pattern Recognition*, 2, II-II (2001).
- [68] H. Huang, K. Sharma, M. Sotiropoulos, and P.F. O'Malley, *Prediction of the output of quantum systems with variational quantum kernels*, *arXiv:2105.09449*, (2021).
- [69] H. Huang, K. Sharma, M. Sotiropoulos, and P.F. O'Malley, *Predicting the properties of molecular systems using quantum kernels*, *Quantum*, 6, 445 (2022).
- [70] L. Liu, J. Bian, P. Rebentrost, and K. Wang, *Learning from distributions based on the discrete logarithm*, *Physical Review Research*, 3(4), 043288 (2021).
- [71] A. Di Pierro and P. Rebentrost, *A quantum support vector machine for small feature spaces*, *arXiv:1810.05867*, (2018).
- [72] A. Di Pierro and M. Incudini, *Quantum machine learning and fraud detection. Protocols, Strands, and Logic*, Springer, Cham, Germany, 139-155 (2021).
- [73] M. Grossi, N. Ibrahim, V. Radescu, R. Loredó, K. Voigt, C. Von Altrock, and A. Rudnik, *Mixed quantum-classical method for fraud detection with quantum feature selection*, *arXiv:2208.07963*, (2022).
- [74] O. Kyriienko and H. Magnusson, *Hybrid quantum-classical classifier with dimensionality reduction for anomaly detection*, *arXiv:2206.16613*, (2022).
- [75] S. Krunić, M. Gastegger, K. Sharma, P. O'Malley, S. Imajo, A. Aspuru-Guzik, and T. E. O'Brien, *Improving the effectiveness of pharmaceutical treatments with quantum kernels*, *arXiv:2202.02108*, (2022).
- [76] E. Peters, C. Pehlevan, C. Campagne-Ibarcq, B. Hacker, A. Chia, J. Bollinger, and S. Lloyd, *A kernel approach to the classification of quantum noise*, *npj Quantum Information*, 7(1), 1-6 (2021).
- [77] Zwitter, Matjaz and Soklic, Milan. *Breast Cancer*. *UCI Machine Learning Repository* (1988). <https://doi.org/10.24432/C51P4M>.